文章编号：1001-9014(XXXX)XX-0001-09

DOI:10.11972/j.issn.1001-9014.XXXX.XX.001

Ridge waveguide SiGe/Si phototransistor with high responsivity

XIE Hong-Yun[1*], XU Zi-Mai[1], JIAO Wei-Zhao[1], MA Yu-Dong[1], LIU Zi-Ming[1], CHEN Liang[2*], NA Wei-Cong[1], ZHANG Wan-Rong[1]

(1. School of Information Science and Technology, Beijing University of Technology, Beijing 100124, China;
2. School of Physics and Electronic Engineering, Taishan University, Taian Shandong 271000, China)

Abstract: Silicon-based phototransistor detectors, offering advantages such as high internal gain, cost-effective and compatibility with CMOS technology, are becoming one of the key devices for large-scale photon integration chip and have significant potential for applications in short-distance optical interconnecting. To relieve its inherent optimization contradiction between responsivity and bandwidth performance, a novel couple ridge waveguide SiGe/Si phototransistor was proposed, in which the carrier transport and the photon propagation were perpendicular and demonstrate the independent optimization on absorption efficiency and operating speed. The optical propagation mode in the SiGe/Si ridge waveguide were analyzed between the single mode and the multiple mode. The geometric parameters of the ridge waveguide to achieve high absorption efficiency were optimized. The ridge waveguide SiGe/Si phototransistor were fabricated using technology compatible with CMOS process platform and achieved a responsivity of 6.4 A/W with the dark current of 10 nA.

Key words: phototransistor, high responsivity, ridge waveguide, photodetector, silicon photonics
PACS:

具有高响应度的脊波导SiGe/Si光电晶体管

谢红云[1*], 徐子脉[1], 焦伟钊[1], 马玉冬[1], 刘子明[1], 陈 亮[2*], 那伟聪[1], 张万荣[1]
(1. 北京工业大学 信息科学技术学院,北京 100124;
2. 泰山学院 物理与电子工程学院,山东 泰安 271000)

摘要:硅基光电晶体管探测器具有内部增益高、成本效益高且与CMOS技术兼容等优势,是大规模光子集成芯片的关键器件之一,在短距离光互连领域具有显著的应用潜力。为缓解其响应度与带宽之间固有的优化矛盾,本文提出了一种新型耦合脊波导SiGe/Si光电晶体管,光波传输方向与载流子传输方向垂直,可以实现吸收效率与工作速度的独立优化。分析了SiGe/Si脊波导中的单模传播模式与多模光传播模式,优化设计SiGe/Si脊波导几何参数实现高的吸收效率。采用与CMOS工艺平台兼容的技术制备了脊波导SiGe/Si光电晶体管,实现了6.4 A/W的响应度和10 nA的暗电流。

关 键 词:光电晶体管;高响应度;脊波导;光探测器;硅光子学

中图分类号:TN364+.3　　**文献标识码**:A

Introduction

The advent of the data-centric era, driven by transformative technologies including 5G/6G communications, large-scale artificial intelligence computing clusters, and the emerging domain of quantum computing [1], has generated an unprecedented demand for data transmission capacity and speed. Conventional electrical interconnects, constrained by inherent bandwidth limitations and high power consumption at scale, are increasingly regarded as a critical bottleneck for future computing systems. Optical interconnects have emerged as the essential successor, offering unparalleled bandwidth and energy efficiency for both long-haul and short-reach communications [2]. This study focuses on short-reach optical interconnect applications utilizing the near infrared band

Foundation items: Supported by the National Natural Science Foundation of China (62475005, 62271014); the Beijing Municipal Natural Science Foundation (4232062, 4192014); the Shandong Province Natural Science Foundation (ZR2021MF077)

Biography: XIE Hong-Yun (1978-), female, Shijiazhuang, Associate Professor, Ph. D, Research area involves semiconductor optoelectronic device and OEIC chip, E-mail: xiehongyun@bjut.edu.cn.

* **Corresponding author**: E-mail: xiehongyun@bjut.edu.cn; tsuchenliang@tsu.edu.cn

(850-980 nm), which is different from O-band and C-band used for long distance communication.

Silicon photonics, leveraging the mature CMOS manufacturing ecosystem, stands as the most promising platform to monolithically integrate optical functionalities, and has established itself as the dominant platform for enabling optical interconnects, where the infrared band (850-980 nm) has become the region of operation. Silicon-based photodetectors, including diode detectors and transistor detectors, are becoming the critical components for the optical receiver. P-i-n photodiodes feature a simple structure, but their poor responsivity struggles to meet high-sensitivity requirements [3-4]. This limitation necessitates the use of complex and power-intensive subsequent transimpedance amplifiers (TIAs) to amplify weak signals, which complicates the receiver architecture and increases overall power budget. APDs possess internal gain and fast response capabilities, but suffer from high noise that degrades their sensitivity [5]. Phototransistor detectors (PTs) integrate light absorption and current gain within a single device [6-7]. This built-in amplification capability positions PT as a compelling candidate to supplant the conventional "photodiode + TIA" combination, thereby simplifying the receiver design and potentially lowering its overall power consumption.

Xie [8] designed and fabricated a high-gain SiGe heterojunction phototransistor (SiGe HPT) on a silicon substrate using a 0.35 um BiCMOS process. They also designed and fabricated SiGe/Si HPTs with varying window positions and sizes, systematically analyzing the impact of lateral parameters on device performance [9]. A. K. Aladim [10] investigated SiGe nanocrystals on SOI substrates for use in photodetectors. This design enhances absorption efficiency through reflection. Tegegne [11] designed and fabricated a SiGe/Si high-power transistor with a sensitivity of 0.805 A/W to meet wireless communication requirements. Subsequently, they developed a SiGe/Si high-power transistor based on low-resistance silicon wafers, achieving a low-frequency response sensitivity of 1.35 A/W [12]. Kostov [13] fabricated p-n-p high-power transistors using a standard 180 nm CMOS process. Experimental data indicated that under 850 nm incident light conditions, the DC response rate of a 100×100 um^2 optical window reached 3.5 A/W. However, the performance of traditional planar or mesa-type HPTs is fundamentally limited by a well-known trade-off: a thick absorption region is required for high quantum efficiency, but this inevitably increases the carrier transit time, thereby limiting the device bandwidth. This performance compromise has been a significant impediment to their widespread adoption in high-speed links.

In this paper, a Si-based coupled ridge waveguide SiGe/Si heterojunction photodetector (CR waveguide SiGe/Si HPT) is proposed. The designed waveguide structure and the way of end-face incidence make the light propagation direction perpendicular to the carrier transport direction and helps to enhance light absorption efficiency and mitigate the trade-off between optical responsivity and response speed.

1 Design of the CR Waveguide SiGe/Si HPT

1.1 Transistor longitudinal structure design

Fig. 1 shows the structure of the proposed CR waveguide SiGe/Si HPT. The coordinate system used for the subsequent modeling and analysis is presented also in Fig. 1. The device design states from the transistor longitudinal structure, namely the epitaxy chip of the CR waveguide SiGe/Si HPT.

An n-type Si with a resistivity of 0.002 – 0.004 Ω·cm is used as substrate, part of which serves as the subcollector of the HPT to make the epitaxy and fabrication easy. The chip epitaxy structure from bottom to top includes: an epitaxial n^--Si collector with a thickness of 700 nm and a doping concentration of 1×10^{17} cm^{-3} grown by low-pressure chemical vapor deposition (LPCVD), a compound base with a thickness of 80 nm, which consists of 40 nm of p^+ Si (2×10^{19} cm^{-3}) and 40 nm of p^+ $Si_{0.8}Ge_{0.2}$ (2×10^{18} cm^{-3}) grown by reduced pressure chemical vapor deposition (RPCVD), an n^+-poly silicon emitter with a thickness of 150 nm and a doping concentration of 2×10^{20} cm^{-3} grown and in situ doped by LPCVD. The designed transistor's epitaxial structure ensures good transistor performance, including high current gain and high transition frequency, which enabling efficient optical absorption, current amplification and high-speed operation when used as a photo-detector.

The SiGe/Si coupled ridge waveguide (CR waveguide) is composed of collector, base, and emitter, as shown in Fig. 1. The direction of waveguide width corresponds to the X-axis, the direction of waveguide length corresponds to the Z-axis, and the direction of waveguide height, perpendicular to the XZ plane, corresponds to the Y-axis. The incident light illuminates on the front end-face and entered into the device, then propagates along the Z direction, and is gradually coupled into the absorption layer and absorbed in there. Although the photo-generated carriers would recombine, most of the photo-generated holes drift to BE junction under the biased electric field and accumulate in base, then lower the BE junction potential barrier. This allows a large number of electrons flow from the emitter to the collector, producing a collector photocurrent much larger than the initial photo-current from photo-generated electrons. The carriers contributing to the collector current mainly transport in the Y direction from emitter to collector or inversely because the collector is forward biased and emitter is grounded. It should be noted that part of the carriers would diffuse in the X direction and Z direction because of the distribution gradient existed there, but those carrier transportations have little even no contribution to collector current. Therefore, the CR waveguide SiGe/Si HPT allows incident light to enter the waveguide from the side end-face and propagate perpendicularly to the carrier movement direction, which provide the opportunity to optimize absorption efficiency and carrier transport times independently and improve optical responsivity without sacrificing operation speed.

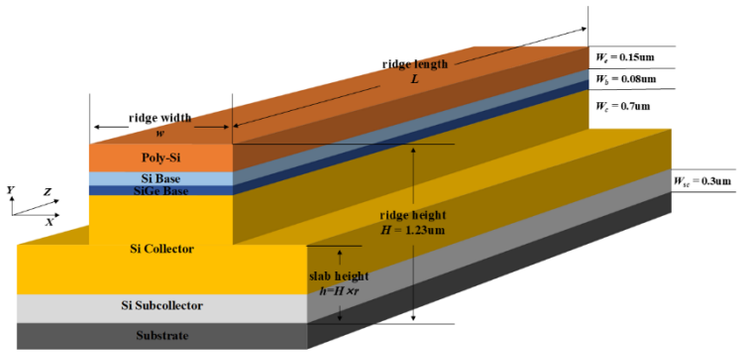

Fig. 1　Structure of the designed coupled ridge waveguide SiGe/Si HPT
图 1　耦合脊波导 SiGe/Si HPT 结构图

1.2　Waveguide structure optimization

A. Propagation modes in the SiGe/Si CR waveguide

The plant light wave in the CR waveguide generally propagate in single-propagation mode or multiple-propagation mode. The waveguide geometrical parameters, including the waveguide width, length ridge height and the slab height are the key factors for the propagation mode of the light wave. Based on the epitaxial layer structure, the ridge height H is 1.23 um (the height of sub-collector is assumed as 300 nm), the slab height h is given by $H\times r$, where r is the slab height factor. The condition for single-mode propagation are analyzed with the effective index method (EMI), which simplify a 3D complex problem into a 2D problems. The EMI method has an acceptable accuracy when each refractive index of the multiple layer is similar to each other, such as the proposed SiGe/Si ridge waveguide. The SiGe/Si multilayer structure is divided from left to right into three regions: region II with the slab height h and an effective refractive index of n_2; region I with the ridge height H and an effective refractive index of n_1; and region Ⅲ with the slab height h and an effective refractive index of n_2, same to the region II, as shown in Fig. 2. Then, a three-layer symmetric planar waveguide was considered with region I as the waveguide layer with thickness of w, region II and region III as the cladding layer. The effective refractive index of the SiGe/Si CR waveguide n_f is achieved through calculating the effective refractive index of this three-layer symmetric planar waveguide. The effective refractive index of each region n_i and the total effective refractive index of the SiGe/Si CR waveguide n_f should satisfy the following conditions [14]:

$$n_{\mathrm{I},m}=\left\{n_f^2-\left[\frac{(m+1)\pi}{kH_{eff}}\right]^2\right\}^{\frac{1}{2}}\quad n_{\mathrm{II},m}=\left\{n_f^2-\left[\frac{(m+1)\pi}{kh_{eff}}\right]^2\right\}^{\frac{1}{2}}\tag{1}$$

where, $m=0,1,2\cdots$ represent the order of the transversal guided mode, $k=2\pi/\lambda$, λ is the wavelength of the incident light, $H_{eff}=H+q$ is the effective height of region I, $h_{eff}=h+q$ is the effective height of region II, $q=\gamma_c/\{k(n_f^2-n_c^2)^{1/2}\}+\gamma_s/\{k(n_f^2-n_s^2)^{1/2}\}$.

To achieve single-mode propagation in the SiGe/Si multilayer CR waveguide, the waveguide geometrical parameters should satisfy two single-mode criterions to ensure that only the fundamental mode can propagate in the transversal direction. The first, the propagation constants of higher-order modes at vertical direction in region I should be smaller than that of fundamental mode at vertical direction in region II and III. The effective refractive index of higher-order transversal modes ($m\geqslant 1$) in the inner ridge (region I) must be less than the effective refractive index of the fundamental mode in the outer ridge region (region II and III) ($n_{1,1}<n_{2,0}$). The second, the higher-order modes at horizontal direction should be cutoff in both the inner ridge region and the outer ridge region. The effective refractive index should satisfy $n_{1,1}=n_{2,0}$. Thus, the single-mode propagation condition for the SiGe/Si multilayer ridge waveguide can be obtained [15-16] as:

$$t<r/(1-r^2)^{1/2}\tag{2}$$

$$\frac{h}{\mathrm{I}H}<\frac{1-q}{2}\tag{3}$$

$$\frac{w}{H}<(1+q)\frac{(h+q)/(H+q)}{\sqrt{1-[(h+q)/(H+q)]^2}}\tag{4}$$

where, $t=w_{eff}/H_{eff}$, $r=h_{eff}/H_{eff}$, $w_{eff}=w+2\gamma_c/\{k(n_f^2-n_c^2)^{1/2}\}$, , n_c is the refractive index of air, and n_s is the refractive index of the substrate. For the TE mode, $\gamma_{c,s}=1$, for the TM mode, $\gamma_{c,s}=(n_{c,s}/n_f)^2$.

Based on the above discussion and the proposed structure, the effective refractive index n_f of the SiGe/Si CR waveguide was calculated to be 3.693. With the refractive index of air n_c being 1 and the effective refractive index of the substrate n_s being 3.65, the geometric structure parameters, including the waveguide width and the slab height, was calculated to satisfy the single-mode propagation for the 850 nm incident light. The region below the curve shown in Fig 3 presents the suitable domain as considering waveguide width and slab height together. When the slab height h are designed as 0.5 um (slab height factors r 0.407) or 1 um (slab height factors r 0.913), corresponding to the ridge section enter into

collector or stop at base, the waveguide width satisfying the single-mode propagation condition are calculated as $w < 0.885$ um or $w < 2.064$ um, respectively.

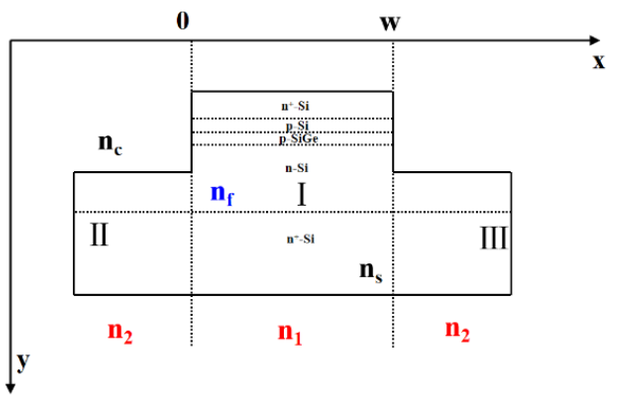

Fig. 2 Effective index analysis of the SiGe/Si multilayer CR waveguide
图 2 SiGe/Si多层耦合脊波导的有效折射率分析

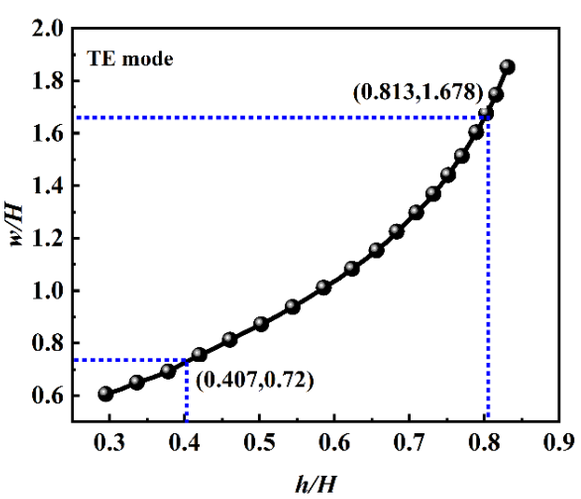

Fig. 3 Single-mode propagation range of the SiGe/Si CR Waveguide
图 3 SiGe/Si耦合脊波导的单模传播范围

Figure. 4(a) and Fig. 4(b) show the TE mode field distributions when $r = 0.407$ with the waveguide width w of 0.8 um and 1.1 um respectively. It is obvious that when $w = 0.8$ um, only the fundamental mode of the TE mode exists in the ridge waveguide. When $w = 1.1$ um, the TE mode in the ridge waveguide includes the fundamental mode and two first-order modes. Fig. 5(a), Fig. 5(b) and Fig. 5(c) show the TE mode field distributions when $r = 0.813$ with the waveguide width w of 2 um, 2.3 um and 8 um respectively. It is evident that when $w = 2$ um, only the fundamental mode of the TE mode exists in the ridge waveguide. When $w = 2.3$ um, the TE mode in the ridge waveguide includes the fundamental mode and one first-order mode. When $w = 8$ um, there are exist the fundamental mode, one first-order mode and other high order modes. It should be pointed out that the actual propagation modes in the SiGe/Si multiple layer waveguide may deviate from the above theoretical analysis because the CR waveguide is the weakly bound waveguide. The coupling effects between different modes becomes seriously when the waveguide geometrical parameters are approaching the critical values of the single-mode condition. The radiation loss at the ridge waveguide boundary and the transmission speed and bandwidth would become worsen in multiple-propagation mode. Meanwhile, the absorption in the CR waveguide to generate electron-hole pairs would have also depend on the propagation modes. The structure design rules for single mode propagation verified in Fig. 4 and Fig. 5 should be comprehensively considered when design the SiGe/Si multilayer CR Waveguide.

The mode field distribution presented in Fig. 4 and Fig. 5 demonstrates that the light power is strongly confined within the BC junction depletion region in the Y-direction due to the designed ridge waveguide, where is the main absorption region in the CR waveguide SiGe/Si HPT. The normalized power intensities in absorption regions shown in Fig. 4 and Fig. 5 are almost equal to each other, both for the single-mode propagation and the multiple-mode propagation. The mode field in X-direction is restricted by the waveguide width and the incident power linearly grow with the waveguide width for the single-mode propagation. However, for the multiple-mode propagation with a wider width, the mode field distribution in X-direction is restricted by itself, then the incident power almost keeps at a certain value, without depending on the waveguide width.

B. Absorption analysis and waveguide structure optimization

Fig. 6(a) and 6(b) show the variation of normalized optical power distribution for the CR waveguides with lengths of 30 um and 50 um respectively. The black, red and blue lines represent the optical power dis-

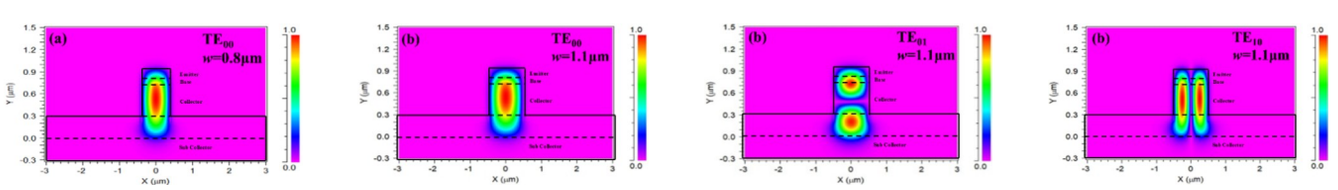

Fig. 4 TE mode field distribution of the SiGe/Si CR waveguide with different waveguide width (slab height factor $r = 0.407$): (a) $w = 0.8$um, (b) $w = 1.1$um
图 4 不同波导宽度下SiGe/Si耦合脊波导的TE模场分布(台面高度因子r = 0.407): (a) w = 0.8um, (b) w = 1.1um

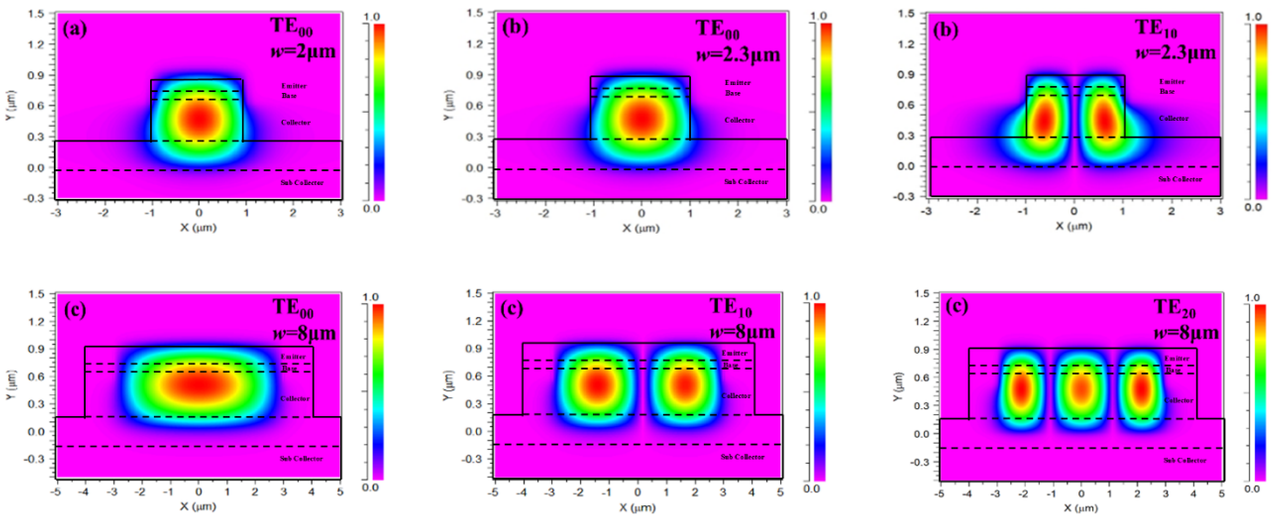

Fig. 5 TE mode field distribution of the SiGe/Si CR waveguide with different waveguide width (slab height factor r = 0.813): (a) w = 2um, (b) w = 2.3um, (c) w = 8um

图 5 不同波导宽度下 SiGe/Si 耦合脊波导的 TE 模场分布(台面高度因子 r = 0.813):(a) w = 2um,(b) w = 2.3um,(c) w = 8um

tributions in collector, base, and emitter, respectively. It can be observed that after the incident light passes through 30 um, the optical power in each layer is nearly zero, indicating that the incident light has been almost completely absorbed. Therefore, the ridge waveguide length should be larger than 30 um to ensure nearly all the incident light absorbed.

Fig. 7 shows the calculated optical carrier generation rate in the CR waveguide SiGe/Si HPT with the length of 30 um under different waveguide widths for the slab height factor of r = 0.407 and r = 0.813 with a developed 3D simulation model based Silvaco TCAD simulation tool. The discussed geometric structure parameters selected here would induce two kinds of light wave propagation mode: the single-mode and the multiple mode. The calculated data show that in the single-mode range (w = 0.4-0.8 um, w = 1.6-2.0 um), the generation rate increases linearly with the waveguide width. In the multiple-mode range (0.9-1.1 um, 2.1-2.3 um, 6-9 um), the generation rate changes little as the waveguide width increases. It is illustrated that once the waveguide width enters the multiple-mode range, further variation in waveguide width does not effectively influence the absorbed optical power, thus the optical carrier generation rate almost keep at a constant.

Fig. 8 presents the calculated responsivity of the CR waveguide SiGe/Si HPT with different waveguide width when the slab height factor are 0.407 and 0.813 respectively, which also consider the same two case of single-mode propagation and the multiple-mode propagation. It can be observed that when r is 0.407, the responsivity increases linearly with the waveguide width within the single-mode range (w = 0.4-0.8 um, r = 0.407) and remains almost constant in the multiple-mode range (w = 0.9-1.1 um, r = 0.407). The maximum responsivity reaches 3.22 A/W under the incident optical power of 3 mW. When r = 0.813, the responsivity increases linearly with the waveguide width within the single-mode range (w = 1.6-2.0 um, r = 0.813). The responsivity remains almost constant in the multi-mode range (w = 2.1-2.3 um, r = 0.813) and the maximum responsivity is 5.27 A/W at P = 3 mW. For the case of r = 0.813 and the waveguide width changing in the range of 6-9 um, the responsivity almost keeps at the constant of 6.1 A/W at P = 3 mW because the light propagates in multiple-mode.

The optical carrier generation rate and the responsivity are sensitive and linear to the waveguide width and waveguide height when the SiGe/Si CR waveguide1 is designed as single-mode propagation. However, both become saturation and insensitive to the waveguide width in the multiple-mode propagation, whatever the slab height factor is 0.407 or 0.813. The reason can be attributed that the field distribution shown in Fig. 4 and Fig. 5 and discussed above. Therefore, the design of the SiGe/Si CR waveguide in the proposed phototransistor would be optional as multiple-mode propagation for the responsivity, especially after considering the fabrication process tolerance.

2 Results and discussions

2.1 Device fabrication and measurement

The designed CR waveguide SiGe/Si HPT was fabricated with sequential processes, including the ridge waveguide preparation, slab mesa fabrication, passivation layer deposition, contact and electrode fabrication, which are compatible with the BiCMOS technology. Fig. 9 presents the SEM photograph of the fabricated CR waveguide SiGe/Si HPT with waveguide length of 30 um, waveguide width of 9 um, and the slab height is about 1-1.05 um (r = 0.813), which realize the multiple-mode propagation for 850nm incident light. The illuminated end-face was prepared on the chip edge to make coupling

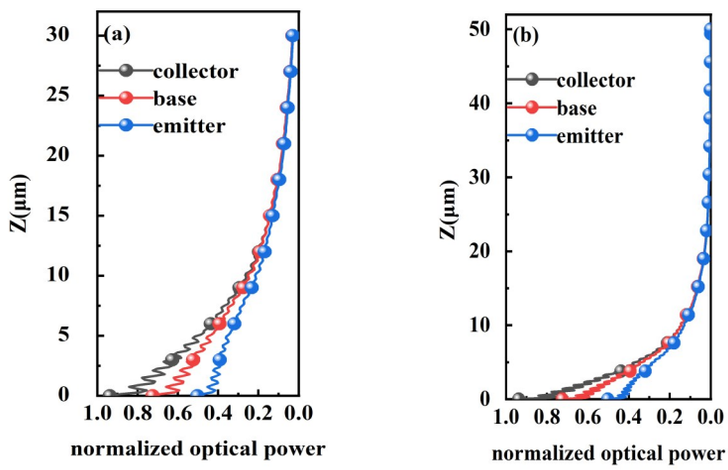

Fig. 6 Optical power variation in emitter, base, and collector with different waveguide lengths: (a) L = 30um, (b) L = 50um
图 6 不同波导长度下发射区、基区和集电区的光功率变化: (a) L = 30um, (b) L = 50um

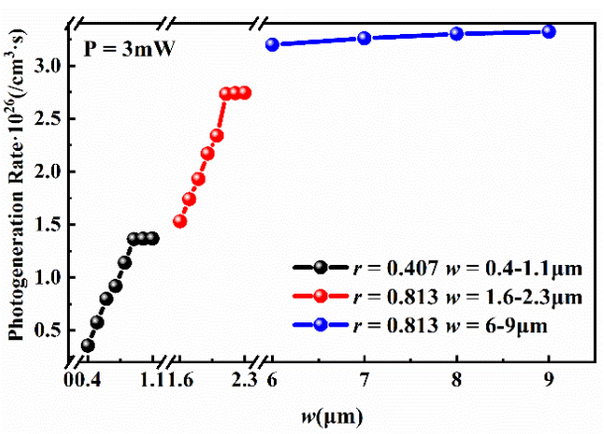

Fig. 7 Optical carrier generation rate of the CR waveguide SiGe/Si HPT with different waveguide widths
图 7 不同波导宽度下耦合脊波导 SiGe/Si HPT 的光载流子产生速率

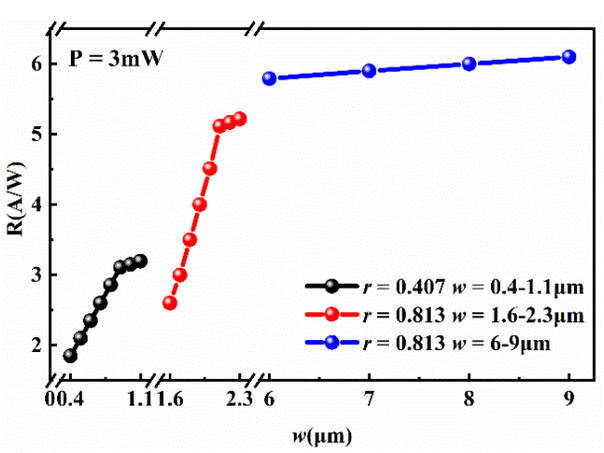

Fig. 8 Responsivity of the CR waveguide SiGe/Si HPT with different waveguide widths
图 8 不同波导宽度下耦合脊波导 SiGe/Si HPT 的响应度

with fiber easily, as shown in Fig. 9.

The DC response is measured with a vacuum probe station, a Keithley 4200 semiconductor parameter analyzer, and a continue wave (CW) laser source with a tail fiber which can provide output light power in Gaussian distribution for 850 nm. The light power arriving at the front end-face of the CR waveguide SiGe/Si HPT is about uW-magnitude after considering the reflection and propagation loss (about 65%), which measured by a light power meter. The maximum light power in our DC testing platform approaches 3. 45 uW.

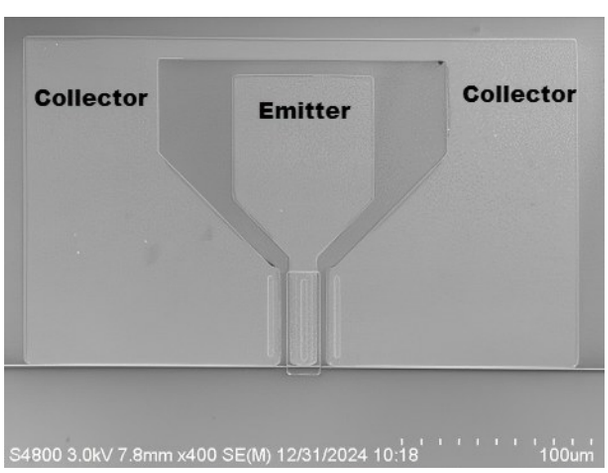

Fig. 9 SEM photograph of the fabricated CR Waveguide SiGe/Si HPT
图 9 耦合脊波导 SiGe/Si HPT 的 SEM 照片

2. 2 DC response

Fig. 10(a) presents the optical output characteristics of the fabricated CR waveguide SiGe/Si HPT when the collector is biased to 1 V, base is floating and emitter is grounded and demonstrates the typical transistor output characteristics. The knee voltage is about 0. 3 V, the

output collector current increase as the incident light power adds from 0 uW to 3. 45 uW gradually and reaches about 22. 25 uA at power of 3. 45 uW. Fig. Fig. 10(b) shows the collector current under different incident power with collector voltage at 0. 1 V, 0. 3 V, 0. 5 V, 0. 7V and 1 V. The responsivity under different incident power and with different biased voltage are calculated from the testing data and shown in Fig. 10(b) and Fig. 10(c), respectively. The responsivity grows quasi-linearly with the incident power in the lower range under all the biased voltages. Meanwhile, the responsivity increases rapidly with the biased voltage and becomes saturation gradually after the knee voltage. It achieves about 6. 4 A/W after 0. 7 V at 3. 45 uW, which is close to the simulated results with the developed 3D model. The dark current of the fabricated CR waveguide SiGe/Si HPT is about 10 nA at the operational voltage of 1-2 V, as shown in Fig. 10(c).

The comparison of the response characteristics between the presented device in this work and other Si-based photodetectors for the similar detection range are shown in Table I [9, 17-22]. Reference [17] and this work present the edge-illuminated SiGe/Si heterojunction phototransisitors with their fabrication method commercial to CMOS/BiCMOS process. Reference [9] and [18] present the top vertical-illuminated SiGe/Si heterojunction phototransisitors based on commercial BiCMOS process. Reference [19], [20], [21] and [22] proposed the PIN/APD photodetector with silicon-nitride optical waveguide. Compared with those reported Si-based detectors, the proposed CR waveguide SiGe/Si HPT photodetector in this work is fabricated using a mature and high cost-performance commercial BiCMOS technology and exhibits almost equal or even higher responsivity under lower biased voltage with a little large dark current.

2. 3　Discussion on RF response

Fig. 11 demonstrates the simulated optical frequency response under different incident power using the de-

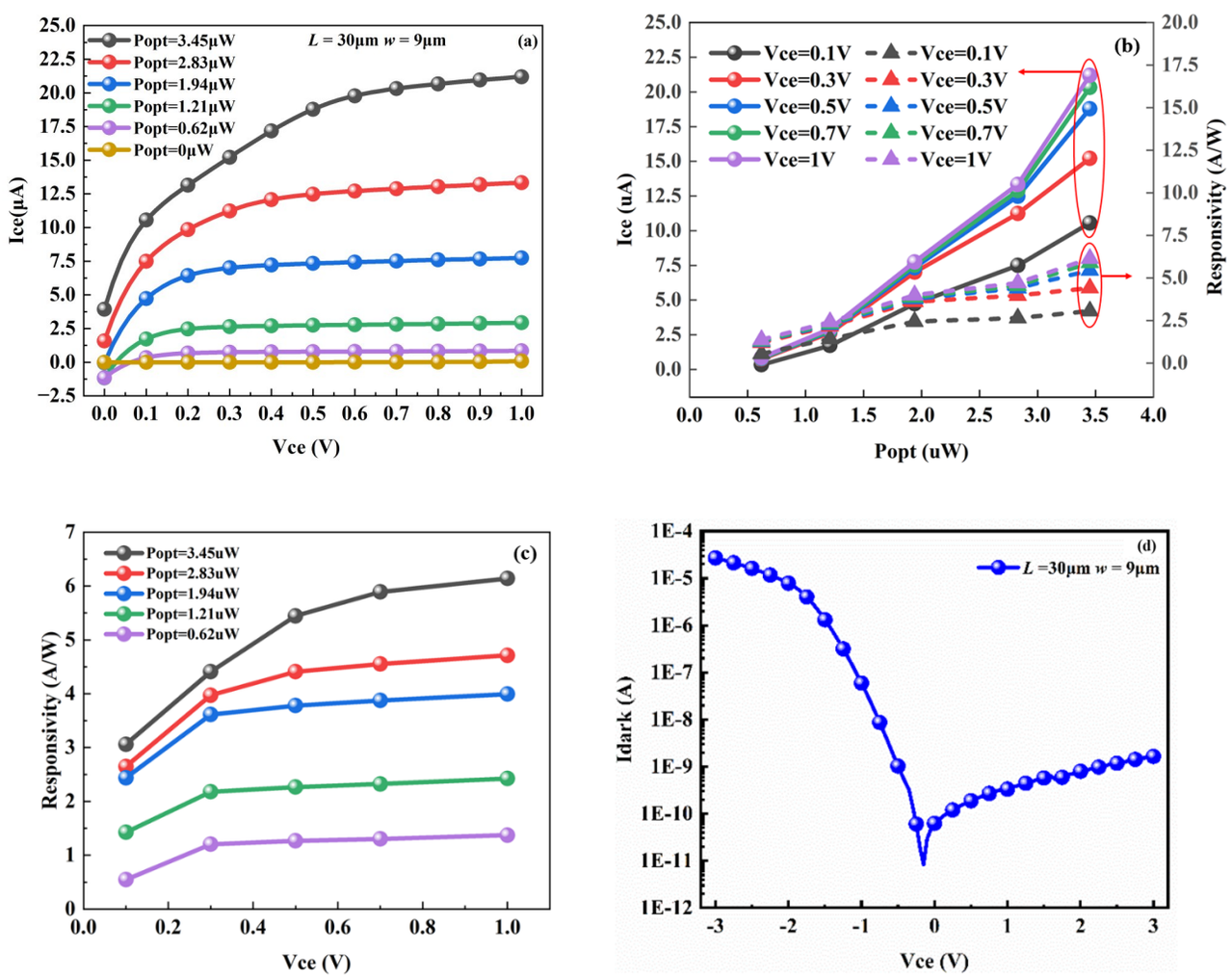

Fig. 10　Optical DC response of the fabricated CR waveguide SiGe/Si HPT: (a) Collector current with different biased voltage, (b) Collector current and responsivity with different incident power, (c) Responsivity with different biased voltage, (d) Dark current.

图 10　耦合脊波导 SiGe/Si HPT 的光学直流响应:(a)不同偏置电压下的集电极输出电流(b)不同注入光功率下的集电极电流和响应度,(c)不同偏置电压下的响应度,(d)暗电流.

Table 1 Response comparison of different Si-based photodetectors under similar detection range
表1 不同硅基光探测器在相似检测范围下的响应比较

Photodetector type	Bias voltage (V)	Size (um^2)	Dark current (A)	Reponsivity (A/W)	Wavelength (nm)	Ref.
SiGe/Si HPT (edge illmunated)	1	9×30	10 n	6.4	850	This work
SiGe/Si HPT (edge illmunated)	0.5	5×5	–	0.45 (opto-microwave responsivity)	850	[17]
SiGe/Si HPT (Top vertical illuminated)	1	20×20	100 p	4.27	850	[9]
SiGe/Si HPT (Top vertical illuminated)	1.6 (ib = 0.2uA)	20×20	–	20.7	900	[18]
graphene gated/Si PIN	−2	1800×1800	0.1−2 p	0.18	390	[19]
SiN/Si Waveguide PIN	−3	11.6×200	107 p	0.19	775	[20]
SiN/Si Waveguide APD	−2	900×16	144 p	>0.2	400−640	[21]
SiN/Si Waveguide PIN/APD	−5.5	200×50	50 p	0.8	685	[22]

veloped 3D simulation model based on the Silvaco TCAD simulation tool. The small signal current gain H_{21} increases with the incident power under small incident power range, such as uW-magnitude. This variation trend is consistent with the measurement DC responsivity and the H_{21} in the lower frequency band achieves its maximum under 10uW. The small signal current gain H_{21} decreases as the incident power adding under larger range, which is attributed that the current saturation under higher incident power [8]. The 3dB-bandwidth enhances gradually with the incident power increasing because of the smaller carrier transit time and RC delay time under the higher incident power and the resulted higher collector current. The 3dB-bandwidth of the proposed CR waveguide SiGe/Si HPT in multiple-mode operation mode with waveguide width of 9 um achieves 1.2GHz and 4.5GHz under 10uW and 3mW, respectively, which indicate that the device can support high speed and high bandwidth application.

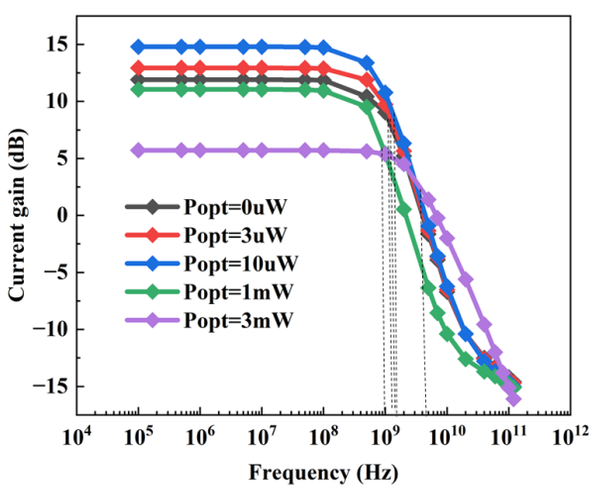

Fig. 11 Simulated RF response under different incident powers
图11 不同入射光功率下的RF光响应仿真

3 Conclusions

A multilayer coupled ridge waveguide SiGe/Si phototransistor (CR waveguide SiGe/Si HPT) was designed and fabricated for optical interconnection application. Unlike vertically top surface illuminated HPTs, the CR waveguide SiGe/Si HPT allows incident light to enter the waveguide from the side end-face and propagate perpendicularly to the carrier movement direction, which provide the opportunity of simultaneous improvement in absorption efficiency and carrier transport speed. The geometric structure parameters, especially the waveguide width and height, are linearly related to the responsivity when the waveguide is designed for single-mode propagation. The responsivity become insensitive to the waveguide width in a multiple-mode couple ridge waveguide, which provide more compatibility to the fabrication process tolerance. The proposed CR waveguide SiGe/Si HPT was fabricated by the technology compatible with the BiCMOS process with the waveguide width of 9 um, waveguide length of 30 um and the slab height about 1 um. The achieved responsivity is 6.4 A/W with the dark current about 10 nA under 850 nm incident light. The RF simulation response demonstrate that the proposed CR waveguide SiGe/Si HPT would be suitable to support high speed and high bandwidth application.

References

[1] Sasiain J, Franco D, Atutxa A, et al. Toward the integration and convergence between 5G and TSN technologies and architectures for industrial communications: A survey [J]. IEEE Communications Surveys and Tutorials, 2025, 27(1): 259-321.
[2] Saxena V, Kumar A, Mishra S, et al. Optical interconnects using hybrid integration of CMOS and silicon-photonic ICs [J]. IEEE Transactions on Circuits and Systems II: Express Briefs, 2024, 71(3): 1632-1637.

[3] Muttlak S G, Kostakis I, Abdulwahid O S, et al. Low-cost InP - InGaAs PIN - HBT-based OEIC for up to 20 Gb/s optical communication systems [J]. IET Optoelectronics, 2019, 13(3): 144-150.
[4] Sharafi F, Orouji A A and Soroosh M. A novel field effect photodiode to control the output photocurrent and fast optical switching [J]. Optical and Quantum Electronics, 2022, 54(3): 171.
[5] Jiang Z B, Yu Y, Wang Y L, et al. High-power Si-Ge photodiode assisted by doping regulation [J]. 2021, Optics Express, 29(5): 7389-7397.
[6] Xie H Y, Shen X T, Ge Y P, et al. A SiGe/Si heterojunction phototransistor for high sensitivity light detection [J]. IEEE Transactions on Electron Devices, 2024, 71(11): 6857-6863.
[7] Nanni J, Tegegne Z G, Viana C, et al. SiGe photo-transistor forlow-cost SSMF based radio-over-fiber applications at 850nm [J]. IEEE Journal of Quantum Electronics, 2019, 55(4): 1-9.
[8] Xie H Y, Xiang Y, Sha Y, et al. A SiGe/Si phototransistor with high FOM of Gain*VA using 0.35-um BiCMOS technology [J]. IEEE Transactions on Electron Devices, 2022, 69(10): 5612-5617.
[9] Xie H Y, Ge Y P, Xu Z M, et al. High responsivity and wide bandwidth SiGe/Si phototransistor for optical interconnection [J]. IEEE Transactions on Electron Devices, 2025, 72(5): 2417-2423.
[10] Aladim A K, Aouassa M, Amdouni S, et al. Photocurrent and electrical properties of SiGe nanocrystals grown on insulator via solid-state dewetting of Ge/SOI for Photodetection and solar cells applications [J]. Vacuum, 2025, 232: 113892.
[11] Tegegne Z G, Viana C, Rosales M D, et al. An 850 nm SiGe/Si HPT with a 4.12 GHz maximum optical transition frequency and 0.805A/W responsivity [J]. International Journal of Microwave and Wireless Technologies, 2017, 9(1): 17-24.
[12] Tegegne Z G, Nanni J, Viana C, et al. Substrate resistivity influence on silicon-germanium phototransistor performance [J]. Electronics Letters, 2019, 55(11): 656-658.
[13] Kostov P, Gaberl W and Zimmermann H. High-speed bipolar phototransistors in a 180nm CMOS process [J]. Optics and Laser Technology, 2013, 46: 6-13.
[14] Pogossian S P, A new approach to determining the waveguide mode index distribution [J]. Optic. Quantum Electron, 1993, 25: 417 - 422.
[15] Pogossian S P, Vescan L and Vonsovici A. The single-mode condition for semiconductor rib waveguides with large cross section [J]. Journal of Lightwave Technology, 1998, 16(10): 1851-1853.
[16] Lousteau J, Furniss D, Seddon A B, et al. The single-mode condition for silicon-on-insulator optical rib waveguides with large cross section[J]. Journal of Lightwave Technology, 2004, 22(8): 1923 - 1929.
[17] Tegegne Z G, Viana C, Polleux J L, et al. Improving the opto-microwave performance of SiGe/Si phototransistor through edge-illuminated structure [C]. Silicon Photonics XI, SPIE, 2016, 9752: 220 - 229.
[18] Thary V, Algani C, Chevalier P, and Polleux J.L. Low-cost and low-voltage Si/SiGe phototransistor with high responsivity at 900nm for microwave photonics applications [J]. IEEE Electron Device Letters, 2025, 46(2): 239-242.
[19] Li, G L Andre N, Huet B, Delhaye T, et al, Enhanced ultraviolet photoresponse in a graphene-gated ultra-thin Si-based photodiode [J], J. Phys. D-Appl. Phys., 52(24): 1-7.
[20] Cuyvers S, Hermans A, Kiewiet M, Goyvaerts J, et al. Heterogeneous integration of Si photodiodes on silicon nitride for near-visible light detection [J], Opt. Lett., 47(4): 937 - 940.
[21] Lin Y D, Yong Z, Luo X S, Azadeh S S, Mikkelsen J C, et al. Monolithically integrated, broadband, high-efficiency silicon nitride-on-silicon waveguide photodetectors in a visible-light integrated photonics platform [J], Nat. Commun., 13[1]: 1 - 7.
[22] Gundlapalli P, Leong V, Ong J R, Ang T Y L, et al. Visible-light integrated PIN avalanche photodetectors with high responsivity and bandwidth [J], J. Lightwave Technol., 41[8]: 2443-2450.